

Chapter 7

Vapor Transport Model Development

Having generated an initial experimental understanding of Directed Vapor Deposition, modeling of vapor transport in a low vacuum gas jet was undertaken using Monte Carlo stochastic methods (Fig. 7.1). The goal of this work was to replicate the experimental results presented in Chapter 5 and provide additional insight into the important processing variables active during DVD material synthesis. For this modeling effort, the Direct Simulation Monte Carlo (DSMC) code of G. A. Bird [148] was utilized to generate velocity vector, pressure, and temperature data for the carrier gas flow at grid points throughout the modeled region. As described in section 2.2.5., the DSMC technique describes the position and momentum of all particles in the fluid system by solving the Boltzmann equation. By tracking binary collisions between a discrete number of representative atoms in the system, the DSMC method is able to replicate the behavior of the much larger number of atoms actually involved in the flowfield.

For the modeling described in this dissertation, the outputs of the DSMC model are used as inputs to a separate bimolecular collision theory (BCT) based model which calculates the mean free path and velocity vector of individual vapor atoms traveling through the car-

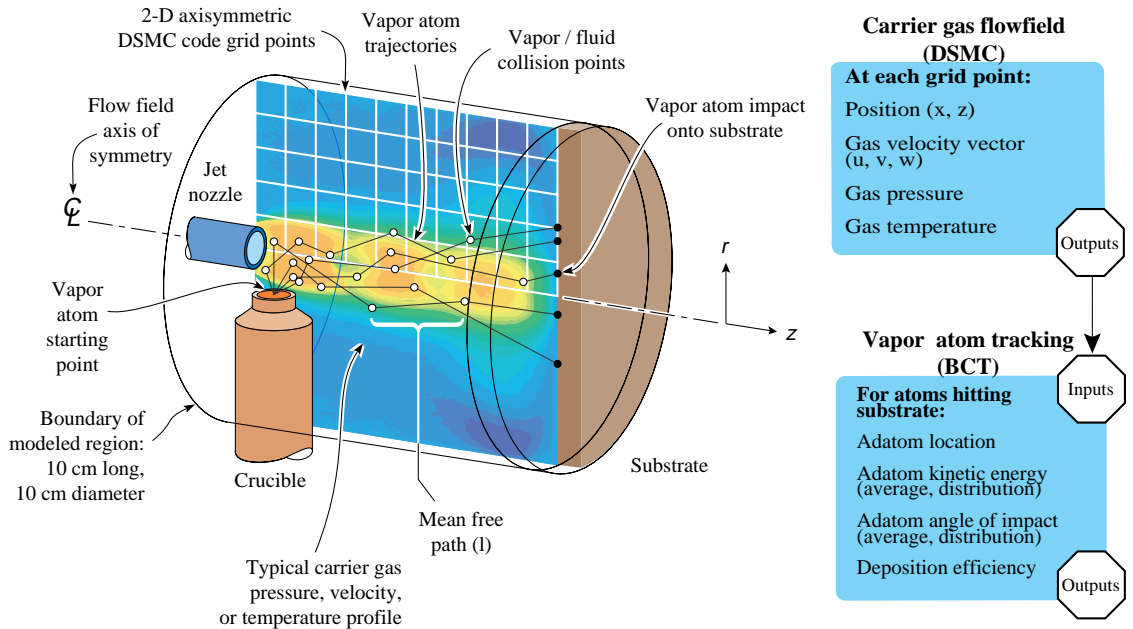


Figure 7.1 Vapor transport modeling of DVD utilizes a Direct Simulation Monte Carlo (DSMC) code, shown here in a two dimensional axisymmetric configuration, to generate information about the carrier gas in the system. A bimolecular collision theory (BCT) model then uses DSMC model outputs to determine vapor atom deposition information.

rier gas flow and which generates deposition efficiency, film thickness, adatom energy, and impact angle data for vapor atoms contacting the substrate. These final vapor transport results are the key inputs necessary for accurate simulations of film microstructure evolution [18 - 22]. These results also facilitate understanding of the visual observations made in section 4.3, help explain experimental observations of microstructure variations with changes in processing conditions [201], and represent a tool which can uncover beneficial system configuration / process condition modifications.

Most calculations for this modeling work were performed on either a 16 node IBM SP2 computer system or two 8 CPU IBM J40 computer systems. Both types of systems are RS6000 class, Unix-based machines. While the DSMC code was not designed to operate

in parallel, it was possible to run the BCT model in a simple parallel mode because it simulated one vapor atom in the carrier gas field at a time. Thus several BCT simulations could be run simultaneously on separate processors using different random number seeds to ensure that the data set generated by each parallel run was unique.

7.1 Direct Simulation Monte Carlo (DSMC) Modeling of the Flowfield

7.1.1. Choice of Discrete Atom Method

Carrier gas flowfield properties can be theoretically explored using either a continuum or discrete atom method, the choice determined by the “degree of rarefaction” of the gas [148]. For moderately dense or dense gases, the continuum method is valid and computationally more efficient than its equally valid discrete atom counterpart. However, at lower gas densities the continuum method breaks down, necessitating solution of the Boltzmann equation rather than the Navier-Stokes equations to obtain flowfield properties [148]. The choice between continuum and discrete is normally made by computing the Knudsen number (Kn), as given in equation (2.20), with Knudsen numbers greater than 0.1 indicating that a discrete atom method must be used.

Computing the mean free path at the nozzle throat for the upper and lower experimental conditions run, ($M_1 = 1.45$, chamber pressure = 0.20 Torr) and ($M_2 = 1.95$, chamber pressure = 4.07), and choosing the nozzle throat diameter (1.27 cm) as the characteristic length L yields $Kn_1 = 0.01$ and $Kn_2 = 0.0003$. These numbers indicate that conditions *at the nozzle throat* can be modeled as a continuum. However, for supersonic flow conditions, as soon as the carrier gas jet enters the chamber, it expands, and the pressure in the center of the jet decreases substantially, perhaps leading to free molecular flow in portions of the modeled volume where continuum techniques will not produce valid results. As Bird

notes [221], “A Knudsen number of 0.1 has traditionally been quoted as the boundary between the continuum and transition regimes, but the characteristic dimension of complex flow fields may be specified in many different ways and the use of an ‘overall Knudsen number’ may be misleading.” To ensure that the entire volume was modeled using a valid methodology, the DSMC method was chosen over continuum methods to simulate the carrier gas flow.

This choice of the DSMC method made possible modeling of conditions where the local Knudsen number reaches or surpasses the continuum limit of 0.1, (e.g. $M_3 = 1.45$, chamber pressure = 0.05 Torr), with the same code used for smaller Knudsen numbers. The discrete atom method is almost certainly more computationally expensive at smaller Knudsen numbers. However, as computer speeds continue to increase, this limitation will cease to confine the method to rarefied gas flows, especially if the DSMC codes are parallelized [222]. Also, since the discrete atom DSMC method utilizes the same general solution techniques as those employed by the BCT model described in section 7.2, use of DSMC should facilitate future integration of the two models into one comprehensive vapor transport process model.

The validity of employing the Direct Simulation Monte Carlo method to model nozzle exhaust flows in low vacuum has been established in recent years by Boyd and others [154, 155, 156], where its primary use has been to understand the interaction of satellite rocket nozzle exhaust plumes with satellite components like solar arrays. The DSMC code used for this modeling work was obtained from Bird’s recent book [148] and modified to the particular geometry and flow conditions of the DVD problem. Fig. 7.2 shows the computational sequence employed by Bird’s DSMC code for flowfield data generation.

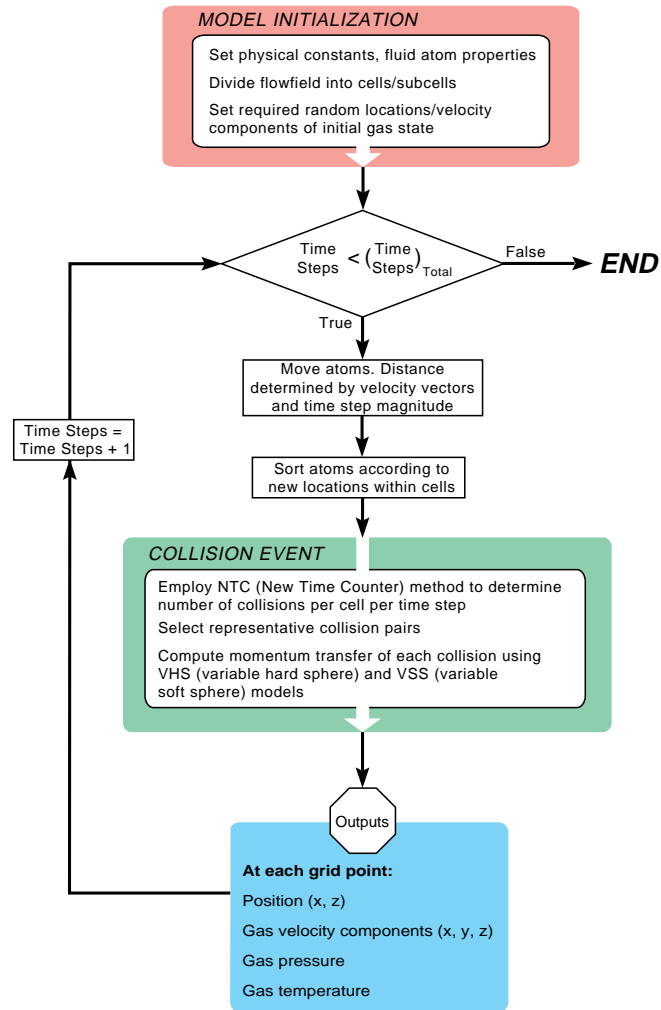


Figure 7.2 The computational sequence of G. A. Bird's Direct Simulation Monte Carlo code for modeling a two-dimensional axisymmetric flowfield.

7.1.2. DSMC Code Adaptation to DVD

Modeling the carrier gas flow with the DSMC code (Appendix C) required the generation of a grid of points at which the pressure (P_c), velocity (U_c), and temperature (T_c) of the carrier gas flow were recorded. The dimensions of the gridded region were based upon the DVD processing space employed for the experimental studies (Fig. 7.3), but, to simplify the modeling process, geometric asymmetries such as the crucible and scanning system

were removed from the modeling configuration, allowing the flow volume to be modeled using a computationally faster two-dimensional axisymmetric rectangular mesh with a line of symmetry about the central (z) axis of the flow. For all simulations, the spacing



Figure 7.3 The locations of the primary DVD components used for the experimental deposition efficiency study define the relative positions of the nozzle, substrate, and crucible source for modeling.

between adjacent gridpoints followed Bird's stipulation that cell dimensions, in flow regions with large macroscopic gradients, should be approximately one third the local mean free path, and time steps over which molecular motion and collisions are uncoupled conformed to Bird's suggestion that they be much less than the local mean collision time [148]. A greater density of gridpoints was placed along the main carrier gas flow line to capture the significant changes in pressure, velocity, and temperature when the flow accelerates out of the nozzle before slowing as it "senses" the substrate's presence and changes direction parallel to the substrate surface (e.g. Fig. 4.12 a)).

Unless noted otherwise, all simulations employed a nozzle radius of approximately 6.35 mm. One-dimensional isentropic¹ flow calculations of a compressible² fluid [125, 146] were used to determine the initial carrier gas pressure, velocity, and temperature at the nozzle throat. The validity of employing isentropic theory for this purpose has been established [155]. Fluid dynamics research has shown that for transonic ($M = 1$) or supersonic flow ($M > 1$), the velocity, pressure, and temperature conditions at the nozzle throat (i.e. the smallest cross-section through which carrier gas flows) always correspond to “choked” or Mach 1.0 conditions. This allows equations (2.18) and (2.19) to be used in combination with the following equation for calculation of the necessary input information [125, 146]:

$$\frac{T_o}{T_d} = 1 + \frac{\gamma - 1}{2} M^2. \quad (7.1)$$

In this equation:

T_o = Upstream temperature (K) and

T_d = Downstream temperature (K).

Thus, if the upstream (mixing chamber) temperature and pressure are 293 K and 667 Pa (5 Torr) respectively, equations (2.18), (2.19), and (7.1) indicate that the model inputs for the nozzle throat should be 220 K, 325 Pa (2.44 Torr), and 873 m/sec if a helium carrier gas is used. While these three equations can be used to predict the carrier gas pressure, velocity, and temperature at the throat and somewhere downstream, they do not describe the change in these properties accurately throughout the two-dimensional axisymmetric free-jet³

¹ isentropic - entropy changes to not occur in the flow.

² compressible - density variations within the flow are nonnegligible.

³ free jet - a gas flow expansion unconstrained by a diverging nozzle.

expansion present in the DVD process. Thus the downstream flowfield's pressure, velocity vector, and temperature values must be determined using the DSMC code.

For DSMC modeling of the DVD flowfield, Bird provides a large number of parameters which can be set to adapt his code to the particular problem under study. Table 5.1 summarizes the important user-configurable parameters and their settings for the DVD simulations in this chapter. An in-depth explanation of each variable can be obtained from [148].

Table 7.1: User-configurable DSMC model parameters

Uniform cell width in x direction	Yes
Uniform cell width in y direction	No
Ratio of cell width at outer y boundary to that at the inner y boundary	3
Number of subcells in x and y directions	2
Weighting factor	Yes
Weighting factor reference radius	0.004
Diffusely reflecting substrate	Yes
Substrate circumferential velocity	0 m/sec
Substrate temperature	300 K
Carrier gas reference diameter (He)	2.33×10^{-10} m
Carrier gas data reference temperature	273 K
Carrier gas molecular mass	6.65×10^{-27} kg
Viscosity temperature power law	0.66
Reciprocal of the variable soft sphere scattering parameter	1

The boundary conditions employed for all DVD simulations were a nozzle, a symmetry axis (along the jet centerline), a substrate, and a low vacuum stream along the other flowfield boundaries (~ 5 m/sec in the positive z direction of Fig. 7.1). The low vacuum stream was designed to simulate the pull of the vacuum pump across the chamber. It also allowed the chamber pressure to be defined in accordance with the experimentally measured chamber pressures of Chapter 4 rather than as a pure vacuum.

The simulated flow conditions were designed to allow reproduction of the experimental deposition efficiency results and thus utilized pure He as the carrier gas for all simulations. The relevant gas parameters were obtained from [148]. In each simulation, the helium carrier gas velocity at the nozzle throat was set to 872 m/sec and the temperature to 220°K (based upon equations (2.19) and (7.1)). Eight background chamber pressures were simulated - 1.33, 4.00, 6.66, 13.3, 26.7, 53.3, 93.3, and 187 Pa (0.01 - 1.40 Torr) - to parallel the experimental results of Chapter 5. For each chamber pressure, three Mach numbers were simulated - Mach 1.45, 1.75, and 1.95. While the total number of atoms simulated was held generally constant (~1,000,000), the number of atoms per cell decreased as the background chamber pressure increased. The effect which this might have on the accuracy of results was of concern. Bird's most recent publication suggests that each cell should contain a minimum of ten to twenty atoms per cell [221]. Examination of the simulated conditions showed that to meet this criterion, the number of atoms simulated for the 187 Pa conditions had to be increased to more than 2 million. Higher chamber pressures were not simulated due to the extreme computational expense of higher pressure runs. Carrier gas flowfield simulations performed with 2,000,000 atoms at 167 Pa required 7-10 days of dedicated computational time on the J40 system. (There were no other users of the system while these calculations were being performed!) Based on Bird's criterion of ten to twenty atoms per cell, at least 3-4 million atoms would have needed to be simulated at a chamber pressure of 333 Pa. It is estimated that each run would then have required 3-4 weeks of uninterrupted, dedicated computational time just to obtain the flowfield. Atom tracking would have required at least 1-2 weeks of multiprocessor computational time if eight or more JJ40 processors could be dedicated to the effort. These calculations were not attempted.

7.2 Bimolecular Collision Theory (BCT) Modeling of Vapor Transport

Modeling of vapor transport was performed using a newly developed stochastic bimolecular collision theory (BCT) model which employs many of the same general binary elastic collision concepts as the DSMC method just described. Written in fortran (Appendix D), the compiled code follows vapor atoms one at a time from the crucible source to the substrate or out of the modeled volume (c.f. Fig. 7.1). During vapor atom transport modeling, vapor atom collisions with individual carrier gas atoms were simulated at intervals determined from mean free path calculations, with each collision event being treated as an elastic, momentum transferring event which changes the velocity vector of the vapor atom. The flow chart of Fig. 7.4 lays out the computational sequence of the BCT model and lists the outputs of the model which simulated a neutral, monoelemental, monatomic carrier gas interacting with a neutral, monoelemental, monatomic vapor atom. To allow comparison between modeling results and the experimental work of Chapter 4, copper was used as the vapor atom for all DVD simulations.

7.2.1. Initial Conditions

The inputs for the BCT model are listed in Table 7.2. The source material temperature during evaporation (T_v) and the exponent (n) for the equation describing the vapor distribution as it leaves the crucible (equation (2.2)) were used at the beginning of the model calculations to determine the initial magnitude and direction of the vapor atom's velocity vector. As described in Chapter 2, studies have shown [7] that controlled e-beam evaporation typically generates evaporant atoms with 0.1 - 0.2 eV of kinetic energy at a source vaporization temperature (T_v) which would lead to an equilibrium vapor pressure of 1 Pa. Using readily available empirical data of vapor pressure versus vaporization temperature for the elements [7, 8], a reasonable value of T_v for the chosen vapor atom was selected as

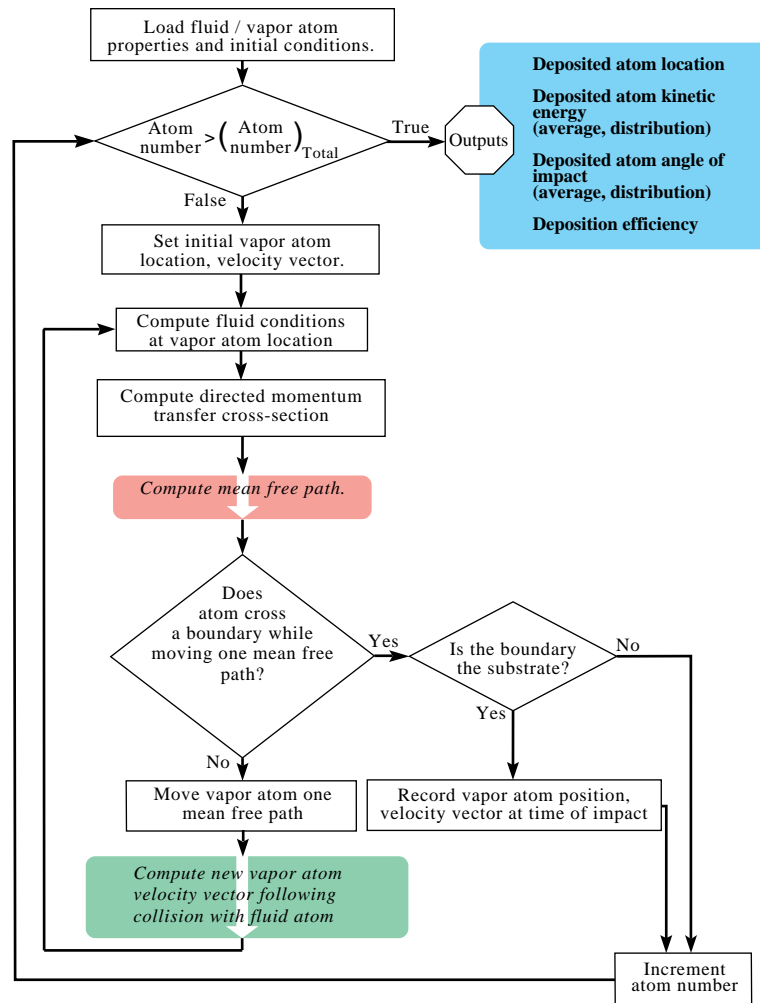


Figure 7.4 The flow chart for the stochastic simulation of vapor atom transport shows the BCT computational sequence.

an input to the model (e.g., for a vapor pressure of 1 Pa, $(T_v)_{\text{Cu}} = 1550$ K). The initial kinetic energy of each vapor atom was then calculated using the Boltzmann temperature equation and the standard kinetic energy equation (equation (2.3)). For copper, the evaporant surface temperature of 1550 K resulted in an initial vapor atom kinetic energy of 0.2 eV, corresponding to a speed of 777 m/sec.

Table 7.2: Required Inputs for Bimolecular Collision Theory Model

Carrier Gas	Vapor Atom
Atomic Number	Atomic Number
Molecular Weight	Molecular Weight
r, z location of DSMC code grid points (Fig. 7.1)	Source material temperature (T_v) at which equilibrium vapor pressure = 1 Pa
U_c, P_c, T_c at DSMC code grid points	Exponent n for the vapor distribution (see equation (2.2))

Having computed the magnitude of the initial vapor atom velocity, the direction of the vapor atom leaving the crucible also had to be determined. As noted in Chapter 2, the density of vapor atoms leaving a high-vacuum e-beam evaporant surface can be described generally by equation (2.2). For the DVD simulations described, the exponent (n) in equation (2.2) was chosen as five based upon experimental measurement of the vapor distribution leaving a crucible in a high vacuum e-beam system (Appendix E)¹. In the newly developed BCT model, the vapor atom's initial direction of travel was selected by generating two random numbers which were used to select the angles θ and α (Fig. 7.5). While the probability density function (PDF) for α was equally weighted across the range 0 to 2π , the PDF for θ was weighted in accordance with the variation of I/I_0 in equation (2.2) across the range 0 to $\pi/2$. Schiller et al. [7] provide the actual PDF which was used to generate the vapor atom distribution (Fig. 7.6):

$$\frac{d_s}{d_{so}} = \frac{1}{\left[1 + \left(\frac{r_s}{h_v}\right)^2\right]^{(n+3)/2}} \quad (7.2)$$

¹ Research by others shows that this simple equation precisely predicts the vapor distribution density at low and moderate e-beam evaporation rates (e.g. from 5 - 10 kW systems), for θ between 0 and $\pi/6$, while slightly overpredicting the density for angles between $\pi/6$ and $\pi/2$ [7].

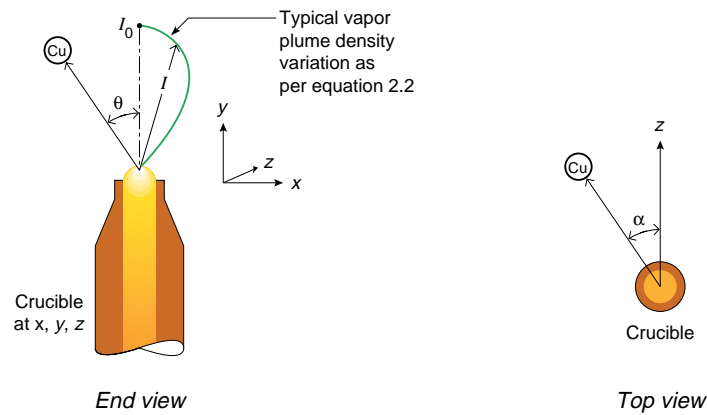


Figure 7.5 Given the magnitude of the initial vapor atom velocity (U_{vi}), selection of θ and α allows the vapor atom velocity vector (U_{vi}) to be described.

where:

- d_s = Local film thickness on a flat substrate,
- d_{s0} = Film thickness for $\alpha = 0$,
- r_s = Distance from midpoint of substrate,
- h_v = Source to substrate separation distance, and
- n = Exponent as used in equation (2.2).

Having computed the initial magnitude and direction of the vapor atom velocity vector, the vapor atom was released into the flowfield for calculation of its subsequent trajectory resulting from carrier gas / vapor atom collisions. The center of the vapor atom source was placed 3.5 cm from the nozzle towards the substrate and 6.4 mm below the modeled volume centerline with the crucible oriented as shown in Fig. 7.1. The radius of the source was chosen as 3.175 mm and vapor atoms had an equal probability of leaving any point on the target surface to simulate evaporation using a fixed e-beam for evaporation.

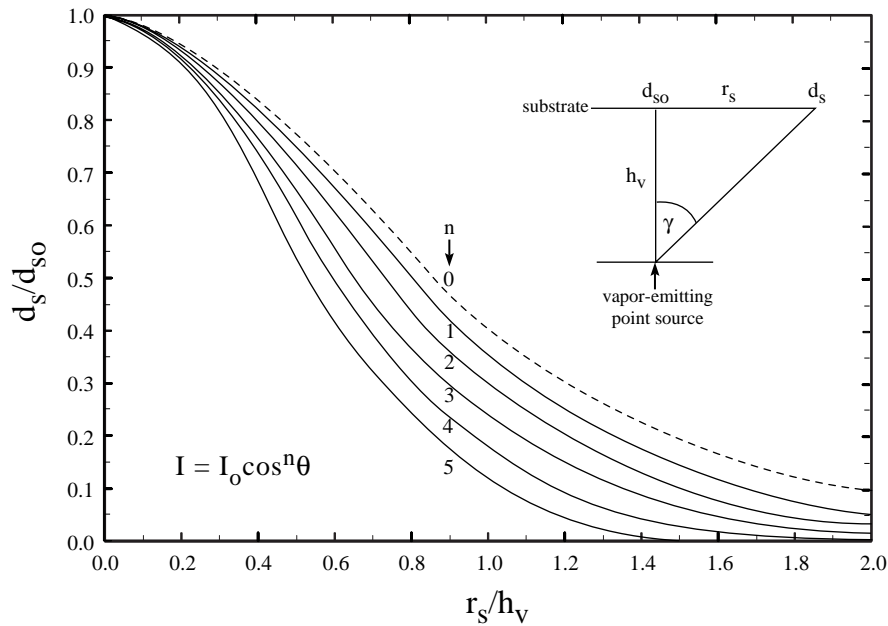


Figure 7.6 Variation of the exponent n in equation (7.2) allows the vapor distribution deposited onto a flat substrate to be rapidly modified.

7.2.2. Distance between collisions

Once the vapor atom was released, it traveled along its constant velocity vector until colliding with a carrier gas atom. McDaniel [134] and Bird [148] have both shown that the point at which such a collision occurs can be determined from a calculation of the atom's mean free path (λ), and, for an atom traveling in a gas whose velocity distribution follows a Maxwell-Boltzmann distribution:

$$\lambda = \frac{RT_c}{\sqrt{2}P_c N_A \sigma_d} \quad (7.3)$$

where R = Universal gas constant (8.3145 J/(mol K)),

T_c = Average carrier gas temperature along vapor atom's path of travel (K),

P_c = Average carrier gas pressure along vapor atom's path of travel (Pa),

$N_A =$ Avogadro's number (6.0221×10^{23} atoms/mol), and

$\sigma_d =$ Directed momentum transfer cross-section for the specific gas/vapor combination.

While equation (7.3) provides the *mean* free path, the distance between collisions actually varies in the real system. This variation is typically described using a Poisson distribution [15, 150]:

$$P_{collision} = \frac{1}{\lambda} e^{-x/\lambda} dx \quad (7.4)$$

to generate the probability of a collision occurring between x and $x + dx$. Equation (7.4) was employed in the BCT model to distribute the free path.

Of the variables included in equation (7.3), σ_d is the most challenging to determine. While T_c and P_c were obtained directly from the output of the DSMC code, the directed momentum transfer cross-section (σ_d) had to be computed using classical two-body collision concepts wherein the final calculated cross-section depended upon the relative kinetic energy of the two atom's involved in a scattering event (E), the impact parameter¹ (b), the center of mass scattering angle (χ), and the angular differential cross-section ($\sigma(\chi)$). Massey [135] notes the applicability of these classical concepts to the two-atom collision event under study here:

“Because of the relatively large masses of gas atoms, these collisions [elastic collisions between gas atoms with energies in the thermal or near-thermal range] are nearly classical. Thus the wavelength of relative motion is short compared with the range of interaction between the atoms, with the exception of only helium atoms at low temperatures [$\sim 1 - 5^\circ\text{K}$]. Apart from this exception, the viscosity

¹ impact parameter - the closest approach that would be achieved by two atoms if their interatomic potentials were not allowed to induce repulsion or attraction.

and diffusion coefficients of gases may be calculated by classical mechanics, provided the atomic interactions are known.”

7.2.3. Calculation of the directed momentum transfer cross-section (σ_d)

Massey and Burhop and others [136, 137, 138] show that the directed momentum transfer cross-section of equation (7.3) is defined by:

$$\sigma_d = 2\pi \int_0^\pi (1 - \cos\chi) \sigma(\chi) \sin\chi d\chi \quad (7.5)$$

where χ = Deflection angle for either atom in center of mass reference frame and
 $\sigma(\chi)$ = Angular differential cross-section.

The angular differential cross-section employed in equation (7.5) is given by [139]:

$$\sigma(\chi) = \frac{b}{\sin\chi} \left| \frac{db}{d\chi} \right| \quad (7.6)$$

where both χ and b are functions of the energy of the atomic interaction event (E). Substitution of (7.6) into (7.5) yields:

$$\sigma_d = 2\pi \int_0^{b_{max}} (1 - \cos\chi) b db \quad (7.7)$$

where: b_{max} = Maximum range of interaction (i.e. maximum effective radius) of atoms involved in collision event.

In equation (7.7) χ is a function of b and of the energy (E) of the specific collision event, making exact solution of σ_d difficult for the dynamic problem under consideration here (i.e., Each collision has a unique energy associated with it, creating a unique functional dependence of χ upon b .) The energy of a collision event is determined by computing the

relative velocity of the two atoms (\vec{U}_r) and a “reduced” mass (m_r) of a single particle interacting with an interatomic potential field (Fig. 7.7). The kinetic energy of the collision event (E) is thus given by equation (2.3). In this equation, the mass is a “reduced” mass:

$$m_r = \frac{m_v m_c}{m_v + m_c} \quad (7.8)$$

where $m_v =$ Vapor atom mass and

$m_c =$ Carrier gas atom mass.

The relative velocity is:

$$\vec{U}_r = \vec{U}_v - \vec{U}_c, \quad (7.9)$$

where $\vec{U}_v =$ Vapor atom velocity vector before collision and

$\vec{U}_c =$ Carrier gas atom velocity vector before collision.

Fig. 7.7 illustrates the functional relationship between b and χ for the universal potential [144] and for various values of E . To simplify solution of equation (7.7), Somekh [15] suggests that a straight-line approximation be made (the dashed lines of Fig. 7.7) in which:

$$\chi(b) = \frac{d\chi}{db} b + \pi \quad (7.10)$$

where: $\frac{d\chi}{db} =$ Constant slope.

Given this approximation, equation (7.5) can be solved to yield:

$$\sigma_d = \pi (b_{max})^2 + \left(\frac{db}{d\chi}\right)^2 \cos\left(\frac{d\chi}{db} b_{max}\right) + \left(\frac{db}{d\chi}\right) b_{max} \sin\left(\frac{d\chi}{db} b_{max}\right) - \left(\frac{db}{d\chi}\right)^2. \quad (7.11)$$

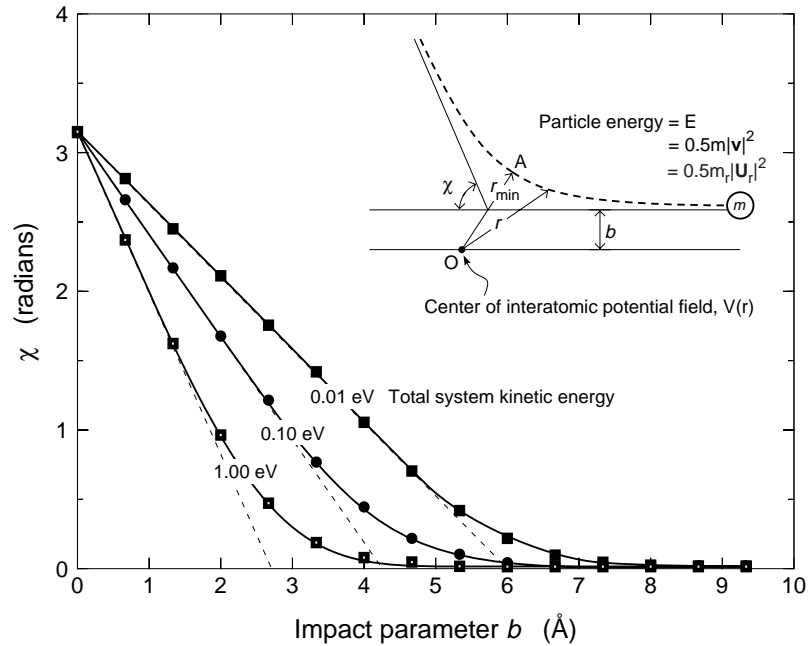


Figure 7.7 The range of impact parameters over which a significant interatomic collision induced deflection takes place is dependent upon the relative kinetic energy of the particles being deflected.

Substitution of appropriate numbers for b_{\max} and $\frac{d\chi}{db}$ into equation (7.11) (e.g. $b_{\max} = 6 \text{ \AA}$, $\frac{d\chi}{db} = -0.5$) reveals that:

$$\sigma_d \cong \pi(b_{\max})^2 \quad (7.12)$$

with the error introduced by neglecting the other terms equal to less than 1.0%. If b_{\max} can now be determined for each collision event, the distance between collisions in the modeled system can be calculated.

7.2.4. Determination of the range of atomic interaction (b_{\max})

Massey and others [135, 136, 139] note that in the classical theory used to describe atom-atom collisions here, b_{\max} is technically infinite because minute angular deflections occur

even for atoms passing one another at large separations (e.g. 10 or more angstroms). To make vapor transport calculations possible, researchers have suggested various cutoff values for b_{\max} , near the intersection of the straight-line approximation with the x-axis (Fig. 7.7). For instance, Somekh [15] has proposed that the selected value of b_{\max} should correspond to 1.1 times the value of b defined by the intersection of the straight line approximation with the x-axis of Fig. 7.7. Due to uncertainty about the influence of small angle deflections upon vapor transport quantities (e.g., vapor atom energy and position), the BCT model employed a different approach in which b_{\max} was chosen to represent the impact parameter corresponding to a chosen minimum “cutoff” deflection angle (e.g., 0.001 radians). The b_{\max} chosen through this method is significantly greater than that proposed by Somekh [15] and others [137].

To solve for the b_{\max} corresponding to a “cutoff” deflection angle, the relationship between χ , b , and E used to generate Fig. 7.7 must be evaluated [137, 139, 141]:

$$\chi = \left| \pi - 2 \int_{r_{\min}}^{\infty} \frac{\frac{b}{r^2}}{\left[1 - \left(\frac{b}{r}\right)^2 - \frac{V(r)}{E} \right]^{1/2}} \right| \quad (7.13)$$

where r = Distance between the atoms,
 r_{\min} = Distance of closest interatomic approach, and
 $V(r)$ = Interatomic potential.

Robinson [137] and Johnson [139] note that integration of equation (7.13) is difficult due to the infinite upper limit and the singularity of the integrand at the point of closest approach r_{\min} . Except for the limited cases in which an analytical solution is possible (e.g. for a Coulomb interaction potential), both authors suggest the use of quadrature schemes

to solve for the deflection angle, with Johnson proposing a simple quadrature in which [143]:

$$\chi(b) \approx \pi \left[1 - \frac{1}{m} \sum_{i=1}^m g(x_i) \right] \quad (7.14)$$

where:

$$g(x_i) \equiv \frac{b}{r_{min}} \left[\frac{1 - x_i^2}{1 - \left(\frac{b}{r_{min}}\right)^2 x_i^2 - \frac{V\left(\frac{r_{min}}{x_i}\right)}{E}} \right]^{1/2} \quad (7.15)$$

and

$$x_i = \cos \left[\frac{(2i-1)\pi}{4m} \right] \quad (7.16)$$

with m being the number of terms used in the calculation¹. (m was chosen as 10 for these calculations. This estimation was found to introduce errors of a few percent into the calculations.)

For the BCT model of DVD vapor transport, the universal potential of Ziegler et al. [144] was chosen to describe the interaction of the carrier gas and vapor atoms:

$$V(r) = \frac{Z_A Z_B e^2}{r} \Phi\left(\frac{r}{a_u}\right) \quad (7.17)$$

¹ Calculation of $\chi(b)$ could also be accomplished, perhaps more quickly, using a so-called Magic Formula (e.g. the Biersack-Haggmark scattering Magic Formula) [144].

where $Z_A =$ Atomic number of carrier gas,

$Z_b =$ Atomic number of vapor atom,

$e =$ Charge on an electron (1 eV),

$a_u =$ Born radius (0.529 Å), and

$$\Phi\left(\frac{r}{a_u}\right) = 0.1818e^{-3.2(r/a_u)} + 0.5099e^{-0.9423(r/a_u)} + 0.2802e^{-0.4029(r/a_u)} + 0.02817e^{-0.2016(r/a_u)} .$$

This purely repulsive potential represents the curve fitting results of theoretically generated potentials to laboratory data for randomly chosen atom pair interactions. Comparison with previously proposed potentials (e.g. Moliere, Lenz-Jensen, and C-Kr) shows that the universal potential produces better agreement between theory and experiment (standard deviation = 5%) when interaction event energies are greater than a few eV [144]. The use of the universal potential in low energy collision events between species like He and Cu (e.g., total collision energy < 1 eV as most often encountered in the DVD system) is somewhat less appropriate due to a need to include precise orbital calculations at these energy levels [144, 205, 206]. Still, Ziegler, et al. [144] note that “the universal potential is valid for nobel gas scattering to potential energies well below 1 eV,” and the current lack of interaction potential data for low energy collisions between species such as He and Cu suggests that use of the universal potential for DVD modeling is a reasonable approach at this time [207, 208].

The solution of equation (7.13) for a specific value of χ_{cutoff} must be done in an iterative manner by choosing a value of b for a given E , finding r_{min} , and then computing χ . Using a standard bisection solution routine [203], b is then increased or decreased from its initial value until b_{max} is determined for the desired cutoff angle χ . Fig. 7.8 shows the relationship between b_{max} and E for three different cutoff values of χ . Because of the log-linear relationship between E and b_{max} for a given value of χ , once χ_{cutoff} is chosen, the specific

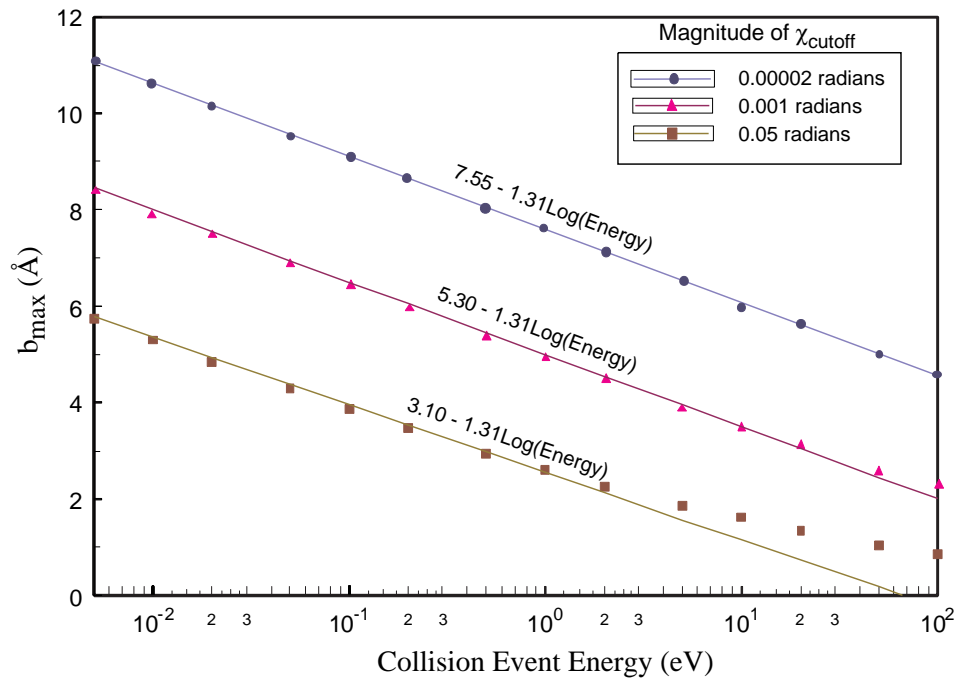


Figure 7.8 For copper-helium interactions, the data points represent solution of equation (7.13) while the lines represent the log-linear curve fits noted above each line.

functional relationship can be determined and the simple function placed inside the BCT code to compute b_{\max} .

During the solution of equation (7.13), r_{\min} is also computed iteratively. Robinson and others [137, 141] point out that r_{\min} is the zero of the radicand in equation (7.13). Thus, the same bisection routine employed to find b_{\max} can be used to compute r_{\min} , given upper and lower bounds on its possible magnitude (e.g., 0 and 15 Å).

Determination of b_{\max} allows σ_d and in turn λ , the mean free path, for any given collision event energy (E) to be calculated. Fig. 7.9 summarizes the steps involved in computing the directed momentum transfer cross-section and thus the vapor atom's mean free path. As the flowchart of Fig. 7.4 notes, if the vapor atom has not left the modeled region or hit the

Compute vapor atom mean free path

- Compute relative velocity of atoms, U_r .
- Compute reduced mass, m_r , of single particle interacting with a potential field.
- Compute energy, $E(U_r, m_r)$, of collision event.
- Determine maximum range of atomic interaction, $b_{\max}(E)$, as per Fig. 7.8.
- Compute the directed momentum transfer cross-section using equation (7.13).
- Compute the mean free path using equation (7.4).

Figure 7.9 A summary of the steps involved in determining the directed momentum transfer cross-section and thus the system's mean free path, λ .

substrate after traversing one mean free path, the change in the magnitude and direction of the vapor atom velocity vector resulting from a collision must now be calculated.

7.2.5. Collision event

Landau and Lifshitz [141] succinctly describe how to solve for the energy and momentum transfer during an elastic two body collision in three dimensions, with the two atoms involved in the collision event changing velocity vector (magnitude and direction) as the result of the interaction. The velocity vectors of the two atoms prior to the collision event (\mathbf{U}_c , \mathbf{U}_v), the mass of the atoms (m_c , m_v), and the form of the interaction potential $V(r)$ represent the three critical inputs to the calculation. For this BCT model, the *average* carrier gas velocity vector (\mathbf{U}_c) provided by the DSMC code for the directions r , θ , and z was modified to generate more realistic vapor velocity vectors following a collision. The car-

rier gas atoms in the actual flow possessed a *distribution* of velocities approximately described by an ellipsoidal drifting Maxwellian (normal) distribution [128]:

$$\phi = n \left(\frac{m_c}{2\pi k T_c} \right)^{3/2} \exp \left(\frac{-m_c [(U_{||} - U_c)^2 - U_{\perp}^2]}{2k T_c} \right) \quad (7.18)$$

where ϕ = Magnitude of the normal distribution for a given value of U_c ,

n = Carrier gas atom number density (atoms/m³)

$U_{||}$ = Carrier gas velocity parallel to primary flow, and

U_{\perp} = Carrier gas velocity perpendicular to primary flow.

Note that equation (7.18) is a modification of the more commonly used Maxwell-Boltzmann equation used to describe a distribution of atomic velocities in a gas at thermal equilibrium [219]:

$$\phi = 4\pi \left(\frac{m_c}{2\pi k T_c} \right)^{3/2} v^2 \exp \left(\frac{-m_c v^2}{2k T_c} \right) \quad (7.19)$$

where v = Molecular speed (m/sec).

Equation (7.18) is designed to take into account the fact that there is a directional flow of gas in the DVD system, and therefore it was used to distribute the velocity vector of the carrier gas atom involved in each collision from the average DSMC value. For simulations of DVD, carrier gas atom velocities were distributed using the inflection points of the bell shaped curve (ϕ) as the standard deviation (ζ) [204]:

$$\zeta = \pm \left[U_{||} - \left(\frac{k T_c}{m_c} \right)^{1/2} \right]. \quad (7.20)$$

As is traditionally done in the literature when computing the results of an elastic collision event, the initial velocity vectors of the two atoms involved were converted from their laboratory reference frame to vectors in the center-of-mass (CM) reference frame, allowing calculation of the momentum and energy change resulting from the collision:

$$\vec{U}_{vcm} = \frac{m_c \vec{U}_r}{m_v + m_c} \quad (7.21)$$

$$\vec{U}_{ccm} = \frac{-m_v \vec{U}_r}{m_v + m_c} \quad (7.22)$$

where \mathbf{U}_{vcm} = Velocity of vapor atom in CM system prior to collision,
 \mathbf{U}_{ccm} = Velocity of carrier gas atom in CM system prior to collision,
 m_v = Vapor atom mass, and
 m_c = Carrier gas atom mass.

In this reference frame, the center of mass is at rest (Fig. 7.10). \mathbf{U}_{vcm} , \mathbf{U}_{ccm} , and the center of mass are all contained within one plane, and the momenta of the two particles are equal in magnitude, opposite in direction. Because the momenta of the two particles are equal in magnitude, the angle of deflection (χ) of the particles in the CM system will also be equal. Landau and Lifshitz note that in the CM system an elastic collision simply rotates the two atoms through an angle χ (change in velocity direction) but does not change their speed (velocity magnitude). If the collision were to occur between two hard spheres with no interatomic potential active between them, then b would equal 0, χ would equal π , and the direction of the two particles would be exactly reversed in the CM system after the collision. However in a system where interatomic potentials are active, a collision occurs whenever the two particles are in the vicinity of one another, resulting in some generally

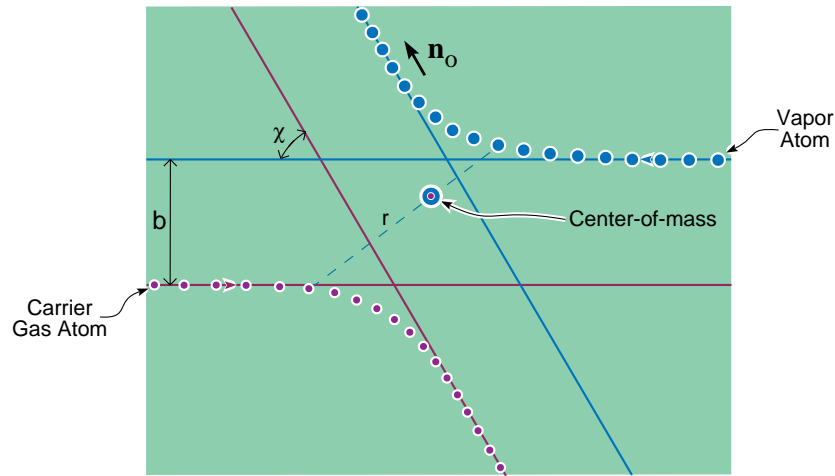


Figure 7.10 If the velocity and position vectors of the vapor and carrier gas atoms are written in a center of mass coordinate system, then the relation between the atoms, the impact parameter of the collision event (b), and the resulting angle of deflection (χ) can be succinctly illustrated.

smaller deflection (less than or equal to π and greater than χ_{cutoff} as noted in section 7.2.4.).

In such an event, an atom which was moving along a direction \mathbf{q} (unit vector) prior to the collision will be moving along a direction \mathbf{n}_o (unit vector) after the collision (Fig. 7.11).

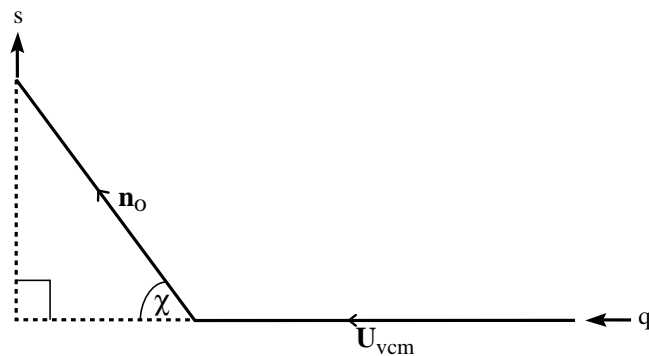


Figure 7.11 The direction of the vapor atom velocity vector in the center-of-mass coordinate system after the collision (\mathbf{n}_o) can be described in terms of the directions \mathbf{q} and \mathbf{s} .

To compute the overall change in vapor atom speed and direction following a collision, the change in direction of the vapor atom in the CM reference frame from \mathbf{q} to \mathbf{n}_o must first be determined. Then the atom's new velocity vector in the CM system (unchanged in magnitude) can be added to the velocity vector of the center of mass to establish the vapor atom's new velocity (speed and direction) in its original laboratory frame of reference. Landau and Lifshitz [141] state that the velocity vector for the vapor atom after a collision is given by:

$$\vec{U}_v = \frac{m_c |\vec{U}_r| \hat{n}_o}{m_c + m_v} + \frac{m_v \vec{U}_v + m_c \vec{U}_c}{m_c + m_v} \quad (7.23)$$

where the first term represents the vapor atom's new CM velocity vector and the second term represents the velocity of the center of mass.

Determination of \mathbf{n}_o involves computing the proportion of the post-collision vapor atom CM velocity vector which lies in the original vapor atom CM velocity vector direction (\mathbf{q}) and the proportion which lies perpendicular to that original direction, along \mathbf{s} . The only requirement for \mathbf{s} (unit vector) is that it be in the plane perpendicular to \mathbf{q} . Although \mathbf{s} has three components of its vector which must be determined (e.g. $a\mathbf{i} + b\mathbf{j} + c\mathbf{k}$), only two governing relationships can be specified about \mathbf{s} since it is not an explicit vector but rather any vector confined to the plane perpendicular to \mathbf{q} . First, \mathbf{s} is perpendicular to \mathbf{q} . Therefore the dot product $\mathbf{q} \cdot \mathbf{s}$ will equal zero. Second, since \mathbf{s} is a unit vector, the sum of the squares of its three components will equal one. Substituting the solution of the first equation (for $a\mathbf{i}$) into the second equation leads to a second order polynomial (for $b\mathbf{j}$) in terms of the third component ($c\mathbf{k}$) of \mathbf{s} and the three components of \mathbf{q} . Since the three components of \mathbf{q} are known, a quadratic equation can be set up to solve for $b\mathbf{j}$ in terms of $c\mathbf{k}$. \mathbf{s} can now be solved for explicitly by selecting $c\mathbf{k}$ subject to two restrictions. First, $c\mathbf{k}$ must be from -1

to 1 since \mathbf{s} is a unit vector. Second, the \mathbf{ck} component randomly chosen between -1 and 1 must create a real number as a part of the root of the quadratic equation for \mathbf{bj} . If the \mathbf{ck} randomly selected between -1 and 1 does not produce a real number, another value for \mathbf{ck} can be randomly chosen from -1 to 1. This process can be repeated until a valid \mathbf{ck} (and thus \mathbf{s}) is produced.

To complete the calculation, the magnitude of \mathbf{b} , in the \mathbf{s} direction, can be randomly chosen between 0 and b_{\max} , and then the CM deflection angle χ can be calculated by the sequence of steps described in section 7.2.4. Once equation (7.23) has been solved, the computational sequence shown in Fig. 7.4 can be repeated until the vapor atom contacts the substrate or crosses one of the other modeling volume boundaries. Fig. 7.12 summarizes the steps involved in computing the change in the vapor atom velocity vector as a result of the collision.

Compute the new vapor atom velocity vector following collision with a carrier gas atom

Distribute average fluid conditions using a Maxwell-Boltzmann distribution.
 Compute relative velocity of atoms, U_r .
 Compute reduced mass, m_r , of single particle interacting with potential field.
 Compute center-of-mass velocity vectors of atoms involved.
 Compute energy, $E(U_r, m_r)$, of collision event.
 Determine maximum range of interaction, $b_{\max}(E)$ as per Fig. 7 .8.
 Randomly choose impact parameter, $b(E)$, between 0 and b_{\max} .
 Compute center-of-mass deflection angle, $\chi(b,E)$.
 Determine center-of-mass direction \mathbf{n}_o for vapor atom after collision.
 Compute new vapor atom velocity vector in laboratory coordinate system.

Figure 7.12 A summary of the steps involved in determining the new direction and speed of a vapor atom after a collision with a carrier gas atom.

7.3 Summary

Having described the design of the vapor transport model developed as a portion of this research program, the accuracy of the method will be assessed in Chapter 8 before being used to study Directed Vapor Deposition in Chapters 9 and 10.